A scheme for lensless X-ray microscopy combining coherent diffraction imaging and differential corner holography

F. Capotondi,[1,*] E. Pedersoli,[1] M. Kiskinova,[1] A.V. Martin,[2] M. Barthelmess,[3] and H. N. Chapman[2,4]

[1]*Fermi, Elettra Sincrotrone Trieste, SS 14 - km 163.5, 34149 Basovizza, Trieste, Italy*
[2]*Centre for Free-Electron Laser Science, Notkestrasse 85, 22607 Hamburg, Germany*
[3]*Photon Science, DESY, Notkestrasse 85, 22607 Hamburg, Germany*
[4]*University of Hamburg, Luruper Chaussee 149, 22761 Hamburg, Germany*
[*]*flavio.capotondi@elettra.trieste.it*

Abstract: We successfully use the corners of a common silicon nitride supporting window in lensless X-ray microscopy as extended references in differential holography to obtain a real space hologram of the illuminated object. Moreover, we combine this method with the iterative phasing techniques of coherent diffraction imaging to enhance the spatial resolution on the reconstructed object, and overcome the problem of missing areas in the collected data due to the presence of a beam stop, achieving a resolution close to 85 nm.

OCIS codes: (100.5070) Phase retrieval; (110.7440) X-ray imaging; (100.3010) Image reconstruction techniques; (090.0090) Holography.

References and links

1. J. Miao, P. Charalambous, J. Kirz, and D. Sayre, "Extending the methodology, of X-ray crystallography to allow imaging of micrometre-sized non-crystalline specimens," Nature **400**(6742), 342–344 (1999).
2. W. Chao, B. D. Harteneck, J. A. Liddle, E. H. Anderson, and D. T. Attwood, "Soft X-ray microscopy at a spatial resolution better than 15 nm," Nature **435**(7046), 1210–1213 (2005).
3. B. Kaulich, P. Thibault, A. Gianoncelli, and M. Kiskinova, "Transmission and emission x-ray microscopy: operation modes, contrast mechanisms and applications," J. Phys. Condens. Matter **23**(8), 083002 (2011) (and references therein).
4. H. N. Chapman, A. Barty, M. J. Bogan, S. Boutet, M. Frank, S. P. Hau-Riege, S. Marchesini, B. W. Woods, S. Bajt, W. H. Benner, R. A. London, E. Plönjes, M. Kuhlmann, R. Treusch, S. Düsterer, T. Tschentscher, J. R. Schneider, E. Spiller, T. Möller, C. Bostedt, M. Hoener, D. A. Shapiro, K. O. Hodgson, D. van der Spoel, F. Burmeister, M. Bergh, C. Caleman, G. Huldt, M. M. Seibert, F. R. N. C. Maia, R. W. Lee, A. Szöke, N. Timneanu, and J. Hajdu, "Femtosecond Diffractive Imaging with a Soft-X-ray Free-Electron Laser," Nat. Phys. **2**(12), 839–843 (2006).
5. D. Shapiro, P. Thibault, T. Beetz, V. Elser, M. Howells, C. Jacobsen, J. Kirz, E. Lima, H. Miao, A. M. Neiman, and D. Sayre, "Biological imaging by soft x-ray diffraction microscopy," Proc. Natl. Acad. Sci. U.S.A. **102**(43), 15343–15346 (2005).
6. A. Barty, S. Marchesini, H. N. Chapman, C. Cui, M. R. Howells, D. A. Shapiro, A. M. Minor, J. C. H. Spence, U. Weierstall, J. Ilavsky, A. Noy, S. P. Hau-Riege, A. B. Artyukhin, T. Baumann, T. Willey, J. Stolken, T. van Buuren, and J. H. Kinney, "Three-dimensional coherent X-ray diffraction imaging of a ceramic nanofoam: determination of structural deformation mechanisms," Phys. Rev. Lett. **101**(5), 055501 (2008).
7. H. N. Chapman, A. Barty, S. Marchesini, A. Noy, S. P. Hau-Riege, C. Cui, M. R. Howells, R. Rosen, H. He, J. C. Spence, U. Weierstall, T. Beetz, C. Jacobsen, and D. Shapiro, "High-resolution *ab initio* three-dimensional x-ray diffraction microscopy," J. Opt. Soc. Am. A **23**(5), 1179–1200 (2006).
8. G. J. Williams, H. M. Quiney, B. B. Dhal, C. Q. Tran, K. A. Nugent, A. G. Peele, D. Paterson, and M. D. de Jonge, "Fresnel Coherent Diffractive Imaging," Phys. Rev. Lett. **97**(2), 025506 (2006).
9. C. M. Günther, B. Pfau, R. Mitzner, B. Siemer, S. Roling, H. Zacharias, O. Kutz, I. Rudolph, D. Schondelmaier, R. Treusch, and S. Eisebitt, "Sequential femtosecond X-ray imaging," Nat. Photonics **5**(2), 99–102 (2011).
10. P. Thibault, V. Elser, C. Jacobsen, D. Shapiro, and D. Sayre, "Reconstruction of a yeast cell from X-ray diffraction data," Acta Crystallogr. A **62**(4), 248–261 (2006).
11. S. Marchesini, "Invited article: a [corrected] unified evaluation of iterative projection algorithms for phase retrieval," Rev. Sci. Instrum. **78**(1), 011301 (2007).

#170906 - $15.00 USD Received 18 Jun 2012; revised 24 Jul 2012; accepted 24 Jul 2012; published 19 Oct 2012

12. X. Huang, J. Nelson, J. Steinbrener, J. Kirz, J. J. Turner, and C. Jacobsen, "Incorrect support and missing center tolerances of phasing algorithms," Opt. Express **18**(25), 26441–26449 (2010).
13. I. McNulty, J. Kirz, C. Jacobsen, E. H. Anderson, M. R. Howells, and D. P. Kern, "High-Resolution Imaging by Fourier Transform X-ray Holography," Science **256**(5059), 1009–1012 (1992).
14. S. Eisebitt, J. Lüning, W. F. Schlotter, M. Lörgen, O. Hellwig, W. Eberhardt, and J. Stöhr, "Lensless imaging of magnetic nanostructures by X-ray spectro-holography," Nature **432**(7019), 885–888 (2004).
15. W. F. Schlotter, R. Rick, K. Chen, A. Scherz, J. Stöhr, J. Lüning, S. Eisebitt, C. Günther, W. Eberhardt, O. Hellwig, and I. McNulty, "Multiple reference Fourier transform holography with soft x rays," Appl. Phys. Lett. **89**(16), 163112 (2006).
16. S. Marchesini, S. Boutet, A. E. Sakdinawat, M. J. Bogan, S. Bajt, A. Barty, H. N. Chapman, M. Frank, S. P. Hau-Riege, A. Szoke, C. Cui, D. A. Shapiro, M. R. Howells, J. C. H. Spence, J. W. Shaevitz, J. Y. Lee, J. Hajdu, and M. M. Seibert, "Massively parallel X-ray holography," Nat. Photonics **2**(9), 560–563 (2008).
17. S. G. Podorov, K. M. Pavlov, and D. M. Paganin, "A non-iterative reconstruction method for direct and unambiguous coherent diffractive imaging," Opt. Express **15**(16), 9954–9962 (2007).
18. M. Guizar-Sicairos and J. R. Fienup, "Holography with extended reference by autocorrelation linear differential operation," Opt. Express **15**(26), 17592–17612 (2007).
19. M. Guizar-Sicairos and J. R. Fienup, "Direct image reconstruction from a Fourier intensity pattern using HERALDO," Opt. Lett. **33**(22), 2668–2670 (2008).
20. D. Gauthier, M. Guizar-Sicairos, X. Ge, W. Boutu, B. Carré, J. R. Fienup, and H. Merdji, "Single-shot Femtosecond X-Ray Holography Using Extended References," Phys. Rev. Lett. **105**(9), 093901 (2010).
21. D. Zhu, M. Guizar-Sicairos, B. Wu, A. Scherz, Y. Acremann, T. Tyliszczak, P. Fischer, N. Friedenberger, K. Ollefs, M. Farle, J. R. Fienup, and J. Stöhr, "High-resolution X-ray lensless imaging by differential holographic encoding," Phys. Rev. Lett. **105**(4), 043901 (2010).
22. http://www.elettra.trieste.it/nanospectroscopy/home/home.html
23. Princeton Instruments camera model PI-MTE.
24. C. Q. Tran, G. J. Williams, A. Roberts, S. Flewett, A. G. Peele, D. Paterson, M. D. de Jonge, and K. A. Nugent, "Experimental measurement of the four-dimensional coherence function for an undulator X-ray source," Phys. Rev. Lett. **98**(22), 224801 (2007).
25. R. Gerchberg and W. Saxton, "A practical algorithm for the determination of the phase from image and diffraction plane pictures," Optik (Stuttg.) **35**, 237–246 (1972).
26. J. R. Fienup, "Phase retrieval algorithms: a comparison," Appl. Opt. **21**(15), 2758–2769 (1982).
27. S. Marchesini, H. He, H. N. Chapman, S. P. Hau-Riege, A. Noy, M. R. Howells, U. Weierstall, and J. C. H. Spence, "X-ray image reconstruction from a diffraction pattern alone," Phys. Rev. B **68**(14), 140101 (2003).
28. S. Bajt, H. N. Chapman, E. A. Spiller, J. B. Alameda, B. W. Woods, M. Frank, M. J. Bogan, A. Barty, S. Boutet, S. Marchesini, S. P. Hau-Riege, J. Hajdu, and D. Shapiro, "Camera for coherent diffractive imaging and holography with a soft-x-ray free-electron laser," Appl. Opt. **47**(10), 1673–1683 (2008).
29. L. Strüder, S. Epp, D. Rolles, R. Hartmann, P. Holl, G. Lutz, H. Soltau, R. Eckart, C. Reich, K. Heinzinger, C. Thamm, A. Rudenko, F. Krasniqi, K. Kühnel, C. Bauer, C. D. Schröter, R. Moshammer, S. Techert, D. Miessner, M. Porro, O. Hälker, N. Meidinger, N. Kimmel, R. Andritschke, F. Schopper, G. Weidenspointner, A. Ziegler, D. Pietschner, S. Herrmann, U. Pietsch, A. Walenta, W. Leitenberger, C. Bostedt, T. Möller, D. Rupp, M. Adolph, H. Graafsma, H. Hirsemann, K. Gärtner, R. Richter, L. Foucar, R. L. Shoeman, I. Schlichting, and J. Ullrich, "Large-format, high-speed, x-ray pnccds combined with electron and ion imaging spectrometers in a multipurpose chamber for experiments at 4th generation light sources," Nucl. Instr. and Meth. A **614**(3), 483–496 (2010).
30. M. J. Bogan, W. H. Benner, S. Boutet, U. Rohner, M. Frank, A. Barty, M. M. Seibert, F. Maia, S. Marchesini, S. Bajt, B. Woods, V. Riot, S. P. Hau-Riege, M. Svenda, E. Marklund, E. Spiller, J. Hajdu, and H. N. Chapman, "Single particle X-ray diffractive imaging," Nano Lett. **8**(1), 310–316 (2008).
31. M. M. Seibert, T. Ekeberg, F. R. N. C. Maia, M. Svenda, J. Andreasson, O. Jönsson, D. Odić, B. Iwan, A. Rocker, D. Westphal, M. Hantke, D. P. DePonte, A. Barty, J. Schulz, L. Gumprecht, N. Coppola, A. Aquila, M. Liang, T. A. White, A. Martin, C. Caleman, S. Stern, C. Abergel, V. Seltzer, J. M. Claverie, C. Bostedt, J. D. Bozek, S. Boutet, A. A. Miahnahri, M. Messerschmidt, J. Krzywinski, G. Williams, K. O. Hodgson, M. J. Bogan, C. Y. Hampton, R. G. Sierra, D. Starodub, I. Andersson, S. Bajt, M. Barthelmess, J. C. H. Spence, P. Fromme, U. Weierstall, R. Kirian, M. Hunter, R. B. Doak, S. Marchesini, S. P. Hau-Riege, M. Frank, R. L. Shoeman, L. Lomb, S. W. Epp, R. Hartmann, D. Rolles, A. Rudenko, C. Schmidt, L. Foucar, N. Kimmel, P. Holl, B. Rudek, B. Erk, A. Hömke, C. Reich, D. Pietschner, G. Weidenspointner, L. Strüder, G. Hauser, H. Gorke, J. Ullrich, I. Schlichting, S. Herrmann, G. Schaller, F. Schopper, H. Soltau, K. U. Kühnel, R. Andritschke, C. D. Schröter, F. Krasniqi, M. Bott, S. Schorb, D. Rupp, M. Adolph, T. Gorkhover, H. Hirsemann, G. Potdevin, H. Graafsma, B. Nilsson, H. N. Chapman, and J. Hajdu, "Single mimivirus particles intercepted and imaged with an X-ray laser," Nature **470**(7332), 78–81 (2011).
32. C. H. Yoon, P. Schwander, C. Abergel, I. Andersson, J. Andreasson, A. Aquila, S. Bajt, M. Barthelmess, A. Barty, M. J. Bogan, C. Bostedt, J. Bozek, H. N. Chapman, J. M. Claverie, N. Coppola, D. P. DePonte, T. Ekeberg, S. W. Epp, B. Erk, H. Fleckenstein, L. Foucar, H. Graafsma, L. Gumprecht, J. Hajdu, C. Y. Hampton, A. Hartmann, E. Hartmann, R. Hartmann, G. Hauser, H. Hirsemann, P. Holl, S. Kassemeyer, N. Kimmel, M. Kiskinova, M. Liang, N. T. D. Loh, L. Lomb, F. R. N. C. Maia, A. V. Martin, K. Nass, E. Pedersoli, C. Reich, D. Rolles, B. Rudek, A. Rudenko, I. Schlichting, J. Schulz, M. Seibert, V. Seltzer, R. L. Shoeman, R. G. Sierra, H.

#170906 - $15.00 USD Received 18 Jun 2012; revised 24 Jul 2012; accepted 24 Jul 2012; published 19 Oct 2012

Soltau, D. Starodub, J. Steinbrener, G. Stier, L. Strüder, M. Svenda, J. Ullrich, G. Weidenspointner, T. A. White, C. Wunderer, and A. Ourmazd, "Unsupervised classification of single-particle X-ray diffraction snapshots by spectral clustering," Opt. Express **19**(17), 16542–16549 (2011).
33. A. V. Martin, N. D. Loh, C. Y. Hampton, R. G. Sierra, F. Wang, A. Aquila, S. Bajt, M. Barthelmess, C. Bostedt, J. D. Bozek, N. Coppola, S. W. Epp, B. Erk, H. Fleckenstein, L. Foucar, M. Frank, H. Graafsma, L. Gumprecht, A. Hartmann, R. Hartmann, G. Hauser, H. Hirsemann, P. Holl, S. Kassemeyer, N. Kimmel, M. Liang, L. Lomb, F. R. N. C. Maia, S. Marchesini, K. Nass, E. Pedersoli, C. Reich, D. Rolles, B. Rudek, A. Rudenko, J. Schulz, R. L. Shoeman, H. Soltau, D. Starodub, J. Steinbrener, F. Stellato, L. Strüder, J. Ullrich, G. Weidenspointner, T. A. White, C. B. Wunderer, A. Barty, I. Schlichting, M. J. Bogan, and H. N. Chapman, "Femtosecond dark-field imaging with an X-ray free electron laser," Opt. Express **20**(12), 13501–13512 (2012).

1. Introduction

After the first demonstration of lensless coherent diffraction imaging (CDI) [1] as a powerful microscopy method, surpassing the resolution limit imposed by the optical elements used in full-field and scanning X-ray microscopy [2, 3], the method has been continuously mastered [4–9]. In CDI the real-space information of the specimen is extracted from the far-field diffraction pattern by an iterative phase retrieval algorithm. The final achievable resolution, using computational methods to obtain the real space image of the object, is governed by the numerical aperture of the pixel-array detector system, by the X-ray wavelength used, and beam transversal coherence. Despite the conceptual simplicity, some technical problems must be overcome during the acquisition of the diffraction patterns and their computational treatment. In particular, the lack of information at low momentum transfer, due to the presence of the beam stop shadow in the experimental data, creates artifacts or stagnation in the reconstruction of the real space object and sometimes *a priori* knowledge of these data are needed to reach fast convergence [10–12]. Fourier transform holography (FTH) is an alternative technique that takes advantage of the beam coherence to reconstruct an off axis image of the sample. In a FTH experiment the scattering wave generated by the investigated object interferes with the one created by a reference, and the recorded Fraunhofer diffraction pattern encodes the relative phase information [13–16]. A single reverse Fourier process is sufficient to obtain the image of the illuminated sample as a spatial convolution of the object and reference amplitudes. Compared to CDI, FTH requires less computation: its resolution, however, is determined by the lateral dimension of key features of the reference scattering structure. The resolution can be improved by decreasing the reference size but at the expense of the reference scattered amplitude, which can worsen the image contrast if the intensity is low for good fringe visibility. Correct balance between the object wave field and the scattering one with sufficient signal to noise ratio for preserving the resolution can be obtained by multiplexing the reference scatterer [15, 16], but this requires complex nano-lithographic processes for sample fabrication.

Here we combine a non-iterative differential holographic method [17–21] with the CDI to overcome the problem of missing data in the phase retrieval algorithm. As recently shown by Zhu *et al.* [21], differential holography utilizing an extended reference is quite robust against the missing data problem, since the differential operator acts as a high pass filter in Fourier space. Consequently, having a low q region of missing data is less critical in this technique with respect to hole holography, since the central region of the diffraction pattern is multiplied by a small number in Fourier space to perform the gradient [17]. Unlike Zhu *et al.* [21] who use Focused Ion Beam (FIB) to define the reference wave encoding the phase to create the off-axis hologram of the object, here we apply a more straightforward approach, using the edges of the Si_3N_4 window supporting the object as multiple scattering references. We find that the edges are sharp enough, in the soft X-ray region, to create an adequate wavefront-modulation between the object-wave and the extended-reference-wave in the diffraction pattern, to define a low resolution hologram of the object that can be used as a starting guess for an iterative reconstruction. Such approach makes the sample preparation easier by avoiding time-consuming FIB nanolithography steps in holographic imaging experiments without affecting the final achievable resolution. This makes the method very appealing for

#170906 - $15.00 USD Received 18 Jun 2012; revised 24 Jul 2012; accepted 24 Jul 2012; published 19 Oct 2012

destructive Free Electron Laser (FEL) CDI experiments, where often several identical replicas of the investigated sample should be prepared to perform ultrafast *"diffract and destroy"* imaging [4].

2. Experimental set up and beam coherence

The experiment was carried out at the Nanospectroscopy beamline (Elettra synchrotron light source) [22]. The X-ray beam from an undulator source was monochromatized by a grating monochromator and using a Kirkpatrick-Baez mirror system was focused to a 150 × 100 μm^2 spot, providing a photon fluency of about 1.3 × 10^{16} ph/s/cm^2.

The experimental set-up is shown in Fig. 1(a): the beam is cleaned from stray radiation and shaped by a 20 μm pinhole placed 89 mm upstream the sample stage, providing a photon flux of 5.2 × 10^{10} ph/s onto the specimen. The diffraction patterns were recorded by a backside illuminated, thermoelectrically cooled, charged coupled device (CCD) camera [23] placed 140 mm downstream the sample (pixel width of 13.5 μm and an array size of 2048 × 2048).

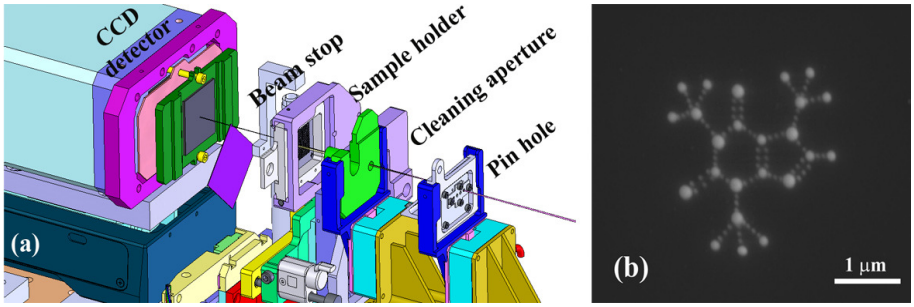

Fig. 1. (a) Experimental set up used in the data collection. (b) SEM image of the test sample, a FIB defined model of the caffeine molecule.

A movable Si wafer is placed between the sample and the CCD to block the direct synchrotron beam. The investigated object is a structural model of a caffeine molecule with dimensions of approximately 3 × 3 μm^2, fabricated by Pt deposition using a FIB on a 30 μm wide Si_3N_4 window chemically etched on a Si wafer (Fig. 1(b)). The "atoms" forming the object are about 110 nm thick with diameters of about 200 nm and 150 nm, as verified by scanning electron microscopy (SEM). The smaller dots, representing the bonds between the "atoms," are 50 nm in diameter and 30 nm thick and the bond length is of about 500 nm.

Before performing the experiment, the coherence of the X-ray beam was characterized, both in the vertical and horizontal directions by a classical Young experiment. A set of two pinholes separated by a distance from 0.5 to 11 μm were used. Figure 2(a) shows the interference pattern recorded by the CCD placed for two pinholes separated by 7 μm and illuminated with photons of 250 eV. The visibility (Fig. 2(b)) of the resulting interference pattern is a measure of the correlation within the wave field incident at the two pinholes. Because of the small pin-hole diameters and the long distance to the detector (140 mm) the far-field conditions are well satisfied and the Fraunhofer limit for the diffraction pattern can be used with a good approximation. Under this assumption the interference pattern *I(P),* observed in a double pinhole experiment at the point *P* of the detector for narrow bandwidth radiation, can be described by the following expression:

$$I(P) = I_1(P) + I_2(P) + \sqrt{I_1(P) \times I_2(P)} \times \left|\gamma_{12}(\tau)\right| \times \cos[\omega \times \tau - \alpha_{12}(\tau)] \qquad (1)$$

Where $I_1(P)$ and $I_2(P)$ are the Airy distributions due to diffraction through the two round pinholes of diameter D, τ is the time delay for the radiation to reach point P from different pinholes, ω is the mean frequency of the incoming radiation, and $\alpha_{12}(\tau)$ is the relative phase.

#170906 - $15.00 USD Received 18 Jun 2012; revised 24 Jul 2012; accepted 24 Jul 2012; published 19 Oct 2012

For narrow bandwidth light, the complex degree of coherence can be approximated by $\gamma_{12}(\tau) = \gamma_{12}(0) \times e^{-i \times \omega \times \tau}$. As a result of the fitting of the Eq. (1) the absolute value of the complex degree of coherence $|\gamma_{12}|$ was obtained for each slit separation for both the horizontal and vertical directions. The red curve in Fig. 2(b) shows the case for a separation between the pin-holes of 7 µm. In according to Tran *et al*. [24] we fit complex degree of coherence as a function of the pinholes separation with a Gaussian, Fig. 2(c), to obtain the coherence length of the illuminating field, defined as the half width at half maximum of the fitting curve. Using the experimental data in Fig. 2(c), we infer a coherence length of the beam of 12 ± 1 µm in the horizontal direction and 11.5 ± 1µm the vertical one. In both directions the coherence length of the beam is greater than the object size allowing us to perform CDI experiment of the object in Fig. 1(b).

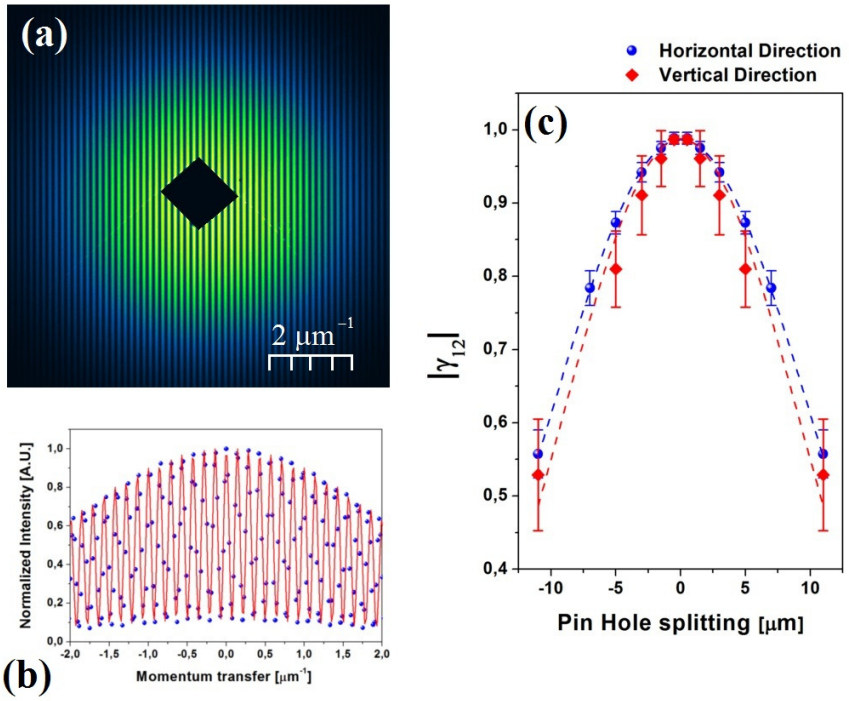

Fig. 2. (a) Far-field diffraction pattern of two pin-holes with an horizontal separation of 7 µm. (b) Young's interference fringes used to measure the coherence properties of the x ray beam at the sample plane, dot experimental data read curve fit using Eq. (1). (c) Modulus of the complex degree of coherence as function of slit separation in the horizontal (circles) and vertical (squares) directions, obtained by fitting to experimental data. The Gaussian fit to the obtained values of $|\gamma_{12}|$ is shown by dashed blue (horizontal direction) and dashed red (vertical direction) lines.

3. Results and discussion

The CDI experiments were carried out acquiring several exposures of duration from 4 s to 300 s, for a total exposure time of 3000 s. The beam stop was placed in different positions for each exposure. Figure 3(a) shows the merged diffraction pattern collected with photon energy of 250 eV, in the exchanged momentum range of ± 13.6 µm^{-1}. The dark parts of the pattern are due to the beam stop and the computational suppression of the diffraction streaks from the edges of the Si_3N_4 supporting window. Our experimental set-up yields a real-space field of view of about 51.4 µm, so the measured diffraction pattern adequately samples the information due to the Si_3N_4 window (30 × 30 µm^2). The encoded information of the Si_3N_4

#170906 - $15.00 USD Received 18 Jun 2012; revised 24 Jul 2012; accepted 24 Jul 2012; published 19 Oct 2012

window is clearly visible on the autocorrelation function of the data in Fig. 3(b), where the image shows the shape of the window and, at the corners, the convolution of the object with the corners. Figure 3(c) illustrates how the autocorrelation changes after the application of a differential filter in the q_x and q_y directions, respectively. Four real space objects, each formed by the caffeine molecule and its twin image, emerge from noise. The inset in the Fig. 3(c) shows a magnification of hologram appearing at the top-right corner. In order to enhance the signal-to-noise ratio and improve the quality of the holographic image obtained with differential holography, we averaged the holograms observed at the corners of the Si_3N_4 window, as illustrated in Fig. 3(d). This image proves that the edges of the Si_3N_4 window are sharp enough to create a low resolution image of the investigated object.

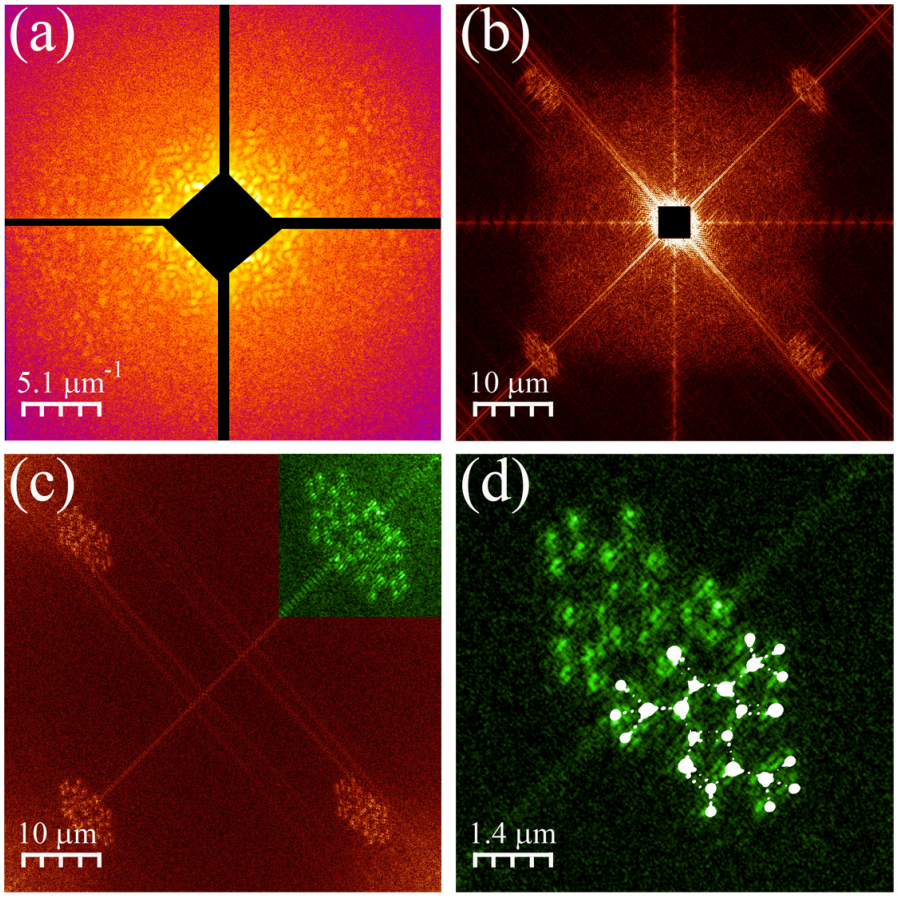

Fig. 3. (a) Far-field diffraction pattern (logarithmic scale) of the model caffeine molecule acquired at 250 eV. (b) Autocorrelation function of the data in (a). (c) Real space holograms, reconstructed applying a two-directional differential filter. The inset is the zoomed top-right corner hologram. (d) Average of the four holograms in (c) which appears almost identical to the superimposed original object (white).

The twin image is decoupled by the real image thanks to the intentional misalignment by about 3 μm in vertical direction of the caffeine molecule with respect to the center of the Si_3N_4 window.

Such low resolution image of the caffeine molecule can be used as initial guess to reconstruct the scattering object using phase retrieval algorithm, filling the low missing data region in Fig. 3(a) and defining the initial phases in the reconstruction and the support.

#170906 - $15.00 USD Received 18 Jun 2012; revised 24 Jul 2012; accepted 24 Jul 2012; published 19 Oct 2012

In Fig. 3(a) the maximum missing data in low momentum transfer q region is about ± 3 μm^{-1}: objects with lateral dimensions greater than 330 nm will have more than one speckle in this region, leading to unconstrained modes [10, 12]. To evaluate the efficacy of low resolution holographic image to guide the reconstruction towards the right solution in the phase retrieval approach, we first performed several attempts to reconstruct the data with different iterative algorithms [11, 25, 26], various input parameters, a "Shrinkwrap" dynamic support constraint [27] and using the autocorrelation function to define the starting support.

Figure 4(a) shows an example of a reconstructed image obtained under the above mentioned attempts. Due to the lack of knowledge of low frequency components, the overestimated initial support introduces several unconstrained Fourier modes in the missing data region [10, 12]: consequently the algorithms are not able to determine the support correctly, creating a meaningless real space image.

A strong improvement in the reconstruction is found if the information coming from hologram is added to guide the algorithm toward the right solution: in this case the iterative process is able to converge to an object having the same shape of the model caffeine molecule (Fig. 4(b)). To estimate the resolution achievable with this combined method, we compare in Fig. 4(c) the radial average of the far-field diffraction pattern (dark line) with the Fourier spectra amplitudes of the two images, obtained with corner holography (dot red line) and phase retrieval (dash blue line). The CDI reconstructed object matches the experimental spectrum up to a momentum transfer of about 6 μm^{-1}, corresponding to a resolution of 85 nm, defined as the half-period of the finest reproduced spatial frequency.

The lower resolution of the holographic image is pointed out in Fig. 4(c) by the enhancement of Fourier amplitude in the region between 0.5 and 2.5 μm^{-1}, which can be ascribed to several factors, namely the partial transparency of the edges, due to the 57.4° tilt of the Si wall after the etching process, the straightness of the edge and the corners roundness. The contribution of the partial transparency of the interface can be taken into account considering the attenuation length of Si at the used wavelength and the tilting angle of the wall. For the present experiment we estimated that within 250 nm from the border the mask becomes completely opaque (transmission less than 1%). An estimation of the overall effect of the sources that limit the resolution in the holographic approach can be inferred by the full field of view of phase retrieval image, where a smoothed square shape of the window borders is expected to appear. However, since the phase retrieval technique imposes a fixed support focused to reconstruct the investigated object in the central part of the image, and a computational suppression of the window diffraction streaks have been applied to the experimental pattern (Fig. 3(a)), the information of the edges is not completely recovered by the CDI algorithm (Fig. 4(d)), and only four bright spots are visible at the corners of the window.

Their full width at half maximum of 350 nm (Fig. 4(e)) gives a measurement of characteristic spatial dimension of the reference scattering structures in holographic approach and consequently an estimation of the hologram resolution. This indicates that most likely the partial transmission of the edges is the main source limiting the resolution of the holographic image.

#170906 - $15.00 USD Received 18 Jun 2012; revised 24 Jul 2012; accepted 24 Jul 2012; published 19 Oct 2012

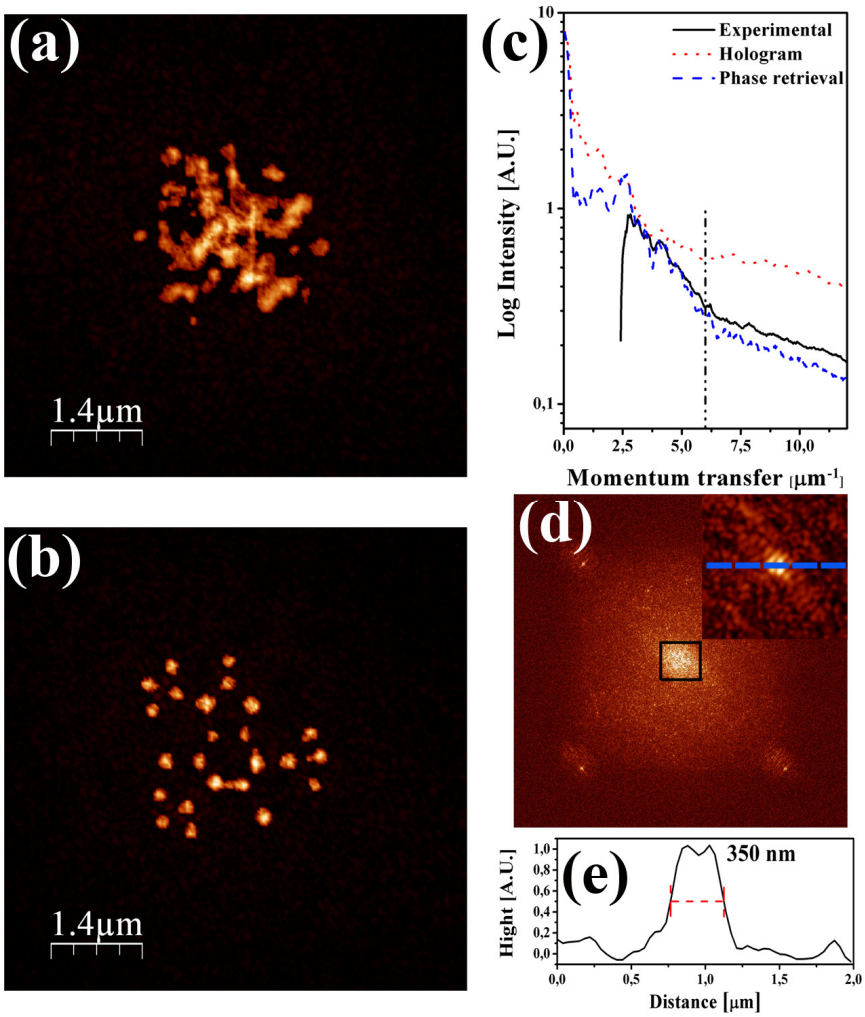

Fig. 4. (a) Reconstructed object using the autocorrelation function to define the initial support in the phase retrieval algorithm. (b) Reconstructed object using the holographic image as initial guess of the phase retrieval algorithm and to define the support. (c) Radial average of the far field diffraction pattern (dark line), Fourier spectrum of holographic object (red dot line) and CDI reconstructed object (blue dash line). (d) Full field view of CDI reconstructed image showing the bright spots at the Si_3N_4 window corners; the color scale is saturated to enhance the contrast of the low scattering features. The square at the center of highlights the zoom part of the reconstructed caffeine molecule shown in (b). Inset shows the zoomed top-right corner. (e) Line profile along the blue dash line inside the inset.

4. Conclusion

In conclusion, we have shown that, using the orthogonal edges of the Si_3N_4 window supporting the illuminated object, a holographic image with sub-micrometric resolution can be obtained, without requiring heavy nano-lithographic sample fabrication. We identify as the main source limiting the resolution of the hologram the smoothness of the window edges, which is determined by the standard etching process used in micro-fabrication. Further steps for improving the holographic resolution can be the use of optical lithography and thin film deposition of high Z metals to define the mask area that provides the reference wave-front. With such more accurate control of the edge sharpness, corner roundness and opacity of the reference structures, better resolution of the image can be achieved. However, the simpler

#170906 - $15.00 USD Received 18 Jun 2012; revised 24 Jul 2012; accepted 24 Jul 2012; published 19 Oct 2012

etching process should be preferred in case low resolution holography is enough to ensure successful reconstruction of high resolution CDI images.

We have also shown that a combination of a non-iterative differential holographic method and iterative phase retrieval can be useful to achieve high resolution images of complex objects even if an extended region of low frequency data is missing. This scheme can be particularly appealing in fixed target CDI experiments using an FEL beam, where the high intensity photon flux imposes the use of a reflecting mirror with a central hole [28] or an *ad hoc* detector configuration [29] that prevents damage to the CCD camera. The ultra-bright FEL radiation also reduces dramatically the exposure time for data collection, making this scheme applicable for dynamic studies in pump-probe experiments. We envision the possibility to decouple the holographic reference mask from the investigated object, implementing this method to CDI experiments where a continuous stream of nano/(micro) particles or living bacteria are injected inside the interaction region with the FEL pulse, to obtain information on the orientation of the hit particle [30, 31]. Within the limitation imposed by the longitudinal coherence length of the beam, the square scattering mask can be inset in the experimental set-up upstream the interaction region between the FEL pulse and the flying object. Such mask will generate a reference wave that interferes with the scattering field of the object to create a hologram on the CCD acquisition plane, increasing the speed of post-processing cataloging and phase retrieving [32, 33].

Acknowledgments

The construction of the apparatus was funded by the Fermi@Elettra project. We are grateful to Andrea Locatelli and Onur Mentes for their help and technical support during instrument commissioning. The authors are in debt with Stefano Marchesini who provided the bitmap of caffeine molecule for FIB deposition.

#170906 - $15.00 USD Received 18 Jun 2012; revised 24 Jul 2012; accepted 24 Jul 2012; published 19 Oct 2012